

Adaptive Materials
How to cite: *Angew. Chem. Int. Ed.* **2021**, *60*, 4358–4367

International Edition: doi.org/10.1002/anie.202011592

German Edition: doi.org/10.1002/ange.202011592

Wavelength-Gated Adaptation of Hydrogel Properties via Photo-Dynamic Multivalency in Associative Star Polymers

Simon Ludwanowski, Oliver Skarsetz, Guido Creusen, Daniel Hoenders, Paula Straub, and Andreas Walther*

Abstract: Responsive materials, such as switchable hydrogels, have been largely engineered for maximum changes between two states. In contrast, adaptive systems target distinct functional plateaus between these maxima. Here, we demonstrate how the photostationary state (PSS) of an E/Z-arylazopyrazole photoswitch can be tuned by the incident wavelength across a wide color spectrum, and how this behavior can be exploited to engineer the photo-dynamic mechanical properties of hydrogels based on multivalent photoswitchable interactions. We show that these hydrogels adapt to the wavelength-dependent PSS and the number of arylazopyrazole units by programmable relationships. Hence, our material design enables the facile adjustment of the mechanical properties without laborious synthetic efforts. The concept goes beyond the classical switching from state A to B, and demonstrates pathways for a truly wavelength-gated adaptation of hydrogel properties potentially useful to engineer cell fate or in soft robotics.

Introduction



Multivalent interactions are of great interest for understanding (bio)chemical systems and designing molecular materials, in which molecules interact by multiple non-covalent bonds.^[1] With respect to the bottom-up design of materials, reversible multivalent interactions are promising in terms of the precise tunability towards external (multiple) stimuli, such as pH,^[2] temperature,^[3] and/or light.^[4] Light is a particularly promising switching mechanism, because of its non-invasive character, high spatial resolution,^[5] and fast response times.^[6]


Hydrogels mimic many of the mechanical properties of soft biological tissues and are widely used for cell culturing, tissue engineering and regenerative medicine.^[7] Here, it is important to note that a property, such as the viscoelastic properties, need to be matched to the requirements of the cells or tissues.^[8] For instance, intestinal stem cell cultures exhibit the highest efficiency of colony formation at a hydrogel stiffness of approximately 1.3 kPa; in contrast, softer and stiffer hydrogels impede cell growth.^[9] An adjustment of the hydrogel properties commonly relies on the type of crosslinks (non-covalent vs. covalent bonds) and on the variation of the crosslinking density.^[10] Supramolecular hydrogels—despite consisting of intrinsically weak interactions—derive tunable viscoelastic characteristics from precisely controlled junctions, length scales and multivalent interactions using molecularly defined components.^[11] Although the understanding of the bottom-up design of such non-covalent materials is rapidly growing, it remains challenging to easily and precisely tune macroscopic characteristics from molecular building blocks and to acquire distinct structure-property relationships.^[12]

There has been great progress in the direction of photo-switchable hydrogels,^[13] ranging from hydrogels based on photoproteins, which dimerize and dissociate upon irradiation with red and far-red light,^[14] to artificial molecular muscles enabling reversible contraction and expansion.^[15] In the latter example, an azobenzene derivative was used as a reversible molecular photoswitch, which interconverts between two conformational states. Azobenzene and its derivatives are likely the most prominent photoswitches with a plethora of examples of switchable materials.^[16] However, these examples typically target maximum switching with the two “best”

[*] S. Ludwanowski, O. Skarsetz, G. Creusen, D. Hoenders, P. Straub, Prof. Dr. A. Walther
A³BMS Lab—Active, Adaptive and Autonomous Bioinspired Materials, Institute for Macromolecular Chemistry, University of Freiburg Stefan-Meier-Straße 31, 79104 Freiburg (Germany)
and
Freiburg Materials Research Center (FMF), University of Freiburg Stefan-Meier-Straße 21, 79104 Freiburg (Germany)
and
Freiburg Center for Interactive Materials and Bioinspired Technologies (FIT), University of Freiburg
Georges-Köhler-Allee 105, 79110 Freiburg (Germany)
P. Straub, Prof. Dr. A. Walther
Cluster of Excellence livMatS @ FIT—Freiburg Center for Interactive Materials and Bioinspired Technologies, University of Freiburg
Georges-Köhler-Allee 105, 79110 Freiburg (Germany)

D. Hoenders, Prof. Dr. A. Walther
A³BMS Lab—Active, Adaptive and Autonomous Bioinspired Materials, Department of Chemistry, University of Mainz
Duesbergweg 10–14, 55128 Mainz (Germany)
E-mail: andreas.walther@uni-mainz.de

 Supporting information and the ORCID identification number(s) for the author(s) of this article can be found under:
 <https://doi.org/10.1002/anie.202011592>.

 © 2020 The Authors. Angewandte Chemie International Edition published by Wiley-VCH GmbH. This is an open access article under the terms of the Creative Commons Attribution Non-Commercial NoDerivs License, which permits use and distribution in any medium, provided the original work is properly cited, the use is non-commercial and no modifications or adaptations are made.

wavelengths to generate the highest photostationary state (*PSS*) accessible of the respective isomer.^[17] Hence, such material concepts target rather classical switching between state A and B to maximize a macroscopic response; that is, a sol-gel transition. Truly adaptive hydrogels with wavelength-gated behavior however go beyond the classical responsive two state material design (from state A to B and back to A).^[18] Such a wavelength-gated adaptation to intermediate switching levels has to the best of our knowledge not been addressed with synthetic photoswitches, but would be desirable for precision engineering of properties. It is interesting to note that the wavelength-dependent activity of drugs in photopharmacology is a related research field.^[19]

Our concept has specific requirements for the used molecular photoswitches. Firstly, the photoresponsive interactions need to be highly reversible without severe photo-induced fatigue. This limits the use of emerging red-shifted light-responsive covalent crosslinkers (e.g., Diels–Alder type cycloadducts), as side-reactions play a role and the cycloreversion is not always feasible.^[20] Secondly, the photoswitch should feature high *PSS*s in both directions, so that one can benefit from its full potential as a switch.^[21] This certainly limits the use of a range of reversible photoswitches.^[22] Thirdly, if thermally self-reverting photoswitches are used, they need a very long thermal stability to truly maintain at a certain intermediate *PSS* after being switched to that state. Considering these requirements, Fuchter and co-workers identified that water-insoluble arylazo-bis(*o*-methylated)pyrazole (AAP) is a particularly promising candidate, because its thermodynamic *E*-isomer isomerizes nearly quantitatively (*PSS* > 98 %) to the metastable *Z*-isomer upon irradiation with UV-light (365 nm) in organic solvents.^[23] The quantitative back switching (*PSS* > 98 %) is either induced by irradiation with green light (532 nm) or occurs very slowly via thermal relaxation in the dark ($\tau_{1/2} \approx 10$ days). Subsequently, Ravoo and co-workers synthesized various water-soluble AAP-PEG (polyethylene glycol) derivatives by modification of the pyrazolyl ring with PEG, and identified that an additional methoxy or iso-propoxy group at the phenyl ring is needed to optimize the *PSS* (*PSS* > 96 %) for aqueous systems while maintaining beneficial long half-lives ($\tau_{1/2} > 6$ days).^[24]

Telechelic associative polymers (TAPs), consisting of a hydrophilic backbone with hydrophobic terminal moieties, can form dynamic and responsive networks in water with transient, sticky network junctions, which allow to control the viscoelastic properties.^[25] Inspired by TAPs but considering the implications of multivalency and wavelength-gated adaptation, we herein report star-shaped PEG polymers (sPEG) with multivalent and photoswitchable AAP end blocks of different compositions. These “sticky” segments form photoswitchable associating linkages based on photo-switchable aromatic donor-acceptor interactions. By exploiting distinct wavelength-gated *PSS*s of the AAP to change the corresponding association strength of the multivalent AAP segments, we will elucidate highly programmable wavelength-adaptive hydrogel properties. We quantify the precise tunability of the *PSS* of a specific AAP unit on the molecular level and transfer this concept to the material scale to derive

comprehensive structure-property relationships. To this end, we characterize the material properties of our AAP-functionalized sPEG (sPEG-AAP_{*x*}) as a function of an increasing number of AAPs (*x*) in the outer segments of the star polymers and characterize in-depth the rheological properties dependent on the incident wavelength (375–545 nm). We demonstrate that the π - π interactions are fully reversible and tunable over the entire range of *PSS*s ($1.7\% \leq PSS_E \leq 96\%$). In contrast to a time-dependent irradiation, reaching a certain *PSS* by different wavelengths leads to a homogenous photo-switching throughout the sample and thus, translates into precisely programmable hydrogel properties. We anticipate that this precise control over the number of interacting stickers as well as over the multivalent interactions is of general relevance to extend the concept of A/B/A responsive materials to adaptive materials with tunable intermediate functional states. This can be of great importance in the field of extracellular matrix materials to provide a new toolbox to accurately control cell fate by external precision manipulation of gel properties.

Results and Discussion

This article focuses on light-adaptation in dynamically associating hydrogels based on multivalent interactions of star-shaped polymers using AAPs as photo-switchable linkers with tunable supramolecular interactions (Figure 1). On the molecular level, AAP exists in two forms—in its thermodynamic *E*- and in its metastable *Z*-isomer (Figure 1 a).^[26] These isomers can be reversibly interconverted by light of different wavelengths (colored curves). Additionally, the metastable *Z*-isomer can undergo thermal relaxation to *E*-AAP after overcoming the activation energy barrier E_A in the dark (dashed curve). Force-field calculations reveal that the *E*-AAP possesses a planar conformation, which favors π - π stacking in aqueous media due to aromatic donor-acceptor interactions of the electron-rich pyrazolyl and the electron-poor phenyl ring (Figure 1 a, Figure S1). In contrast, the *Z*-isomer of AAP features a twisted conformation and a higher dipole moment, which impede π - π stacking in water.^[24c] We verified the calculations of the aromatic donor-acceptor interactions via 2D NOESY (Nuclear Overhauser Effect Spectroscopy) NMR experiments and confirmed that the aromatic donor-acceptor interactions of the *E*-isomer are distinctly stronger than the ones of the *Z*-isomer (Figure S2). Since π - π interactions are individually weak, we embedded them into a multivalent system (Figure 1 c). To this end, we chain-extended sPEG to prepare multivalent building blocks with a defined number of AAPs in an otherwise solubilizing block (synthetic details below; Scheme 1). We emphasize that proper design on the polymer level is important to assure well-dissolved systems and absence of strong solubility transitions.

The idea towards light-adaptive systems stems from multivalent interactions which can be tuned in the material by only switching a part of the AAP units in a highly selective manner to precisely modulate their interactions. This in fact means that the two-state system of an individual AAP (*E/Z*;

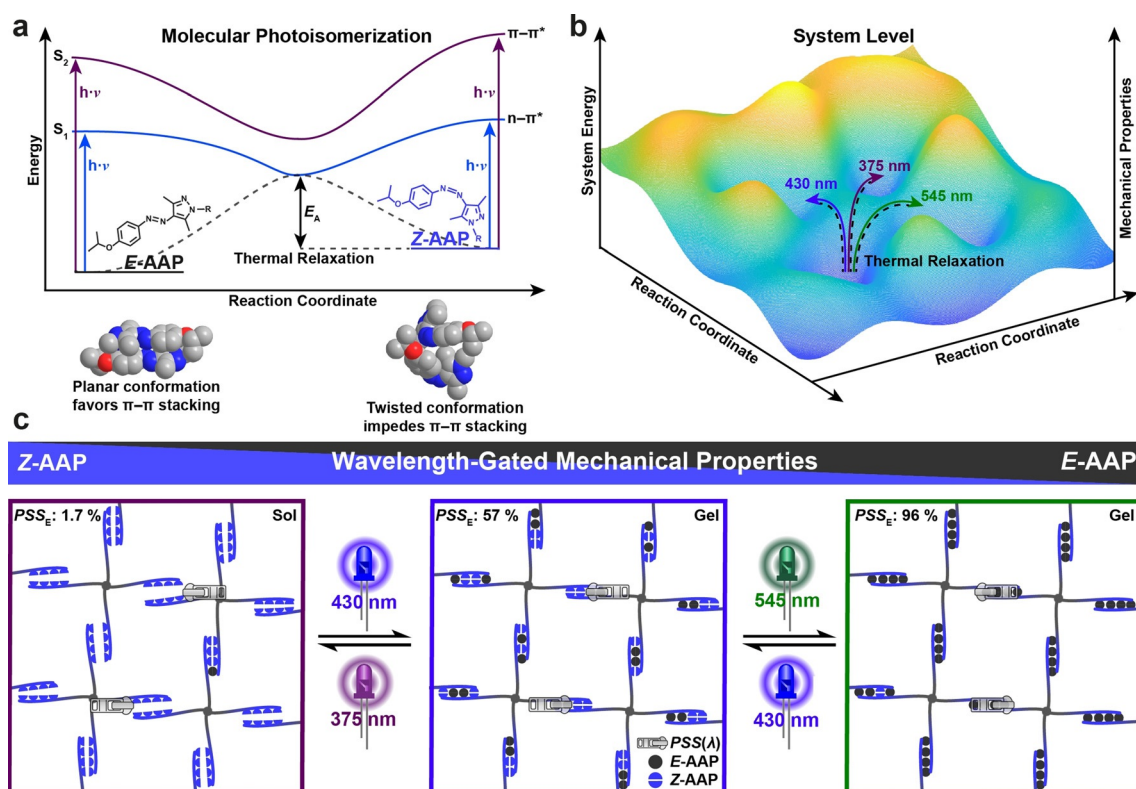
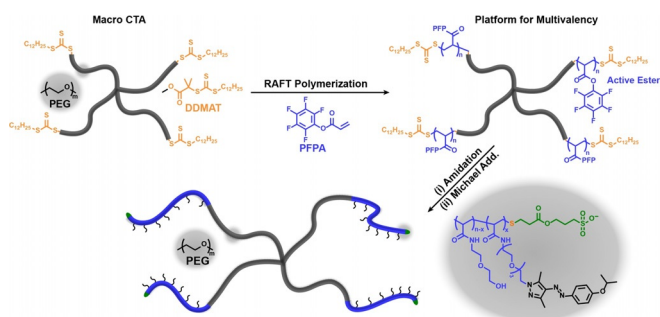


Figure 1. Schematic illustration of precisely and reversibly adaptable multivalent hydrogels based on star-shaped associative polymers. a) Energy landscape during photoisomerization and thermal relaxation of an individual AAP. On the molecular level, AAP possesses two forms, which are converted into each other by light of different colors or via thermal relaxation in the dark. The planar E -AAP favors π - π stacking in water and acts as a dynamic crosslinker (sticker) in the resulting network. In contrast, the Z -AAP impedes π - π stacking due to its twisted conformation and its higher dipole moment. b) 3D energy surface, which correlates the system energy to the mechanical properties of the system. Each $PSS(\lambda)$ represents a local minimum on the energy landscape with a deep metastability due to the long thermal half-lives of AAPs. c) Wavelength-gated mechanical properties. The degree of association of the polymer strands depends on the PSS of E - vs. Z -AAP, ranging from nearly no interaction (left, sol) to nearly full association (right, gel). The PSS_E is a function of the wavelength λ , which allows to engineer the mechanical properties of hydrogels by light of different wavelengths.



Scheme 1. Synthesis and functionalization of chain-extended sPEG-*b*-pPFPAs₁ to obtain dynamically associating, multivalent, and light-adaptive networks.

Figure 1 a) is extended on a system level to many different metastable energy states that can be selectively addressed by different wavelengths (Figure 1 b). We will show below that if a system is irradiated for instance with 375 nm, 430 nm, or 545 nm (colored arrows; Figure 1 b), each wavelength will drive the system into a specific $PSS(\lambda)$ in the energy landscape with a certain ratio of E/Z -isomers. Correspondingly, we show

that the mechanical hydrogel properties (2nd z-axis; Figure 1 b) are directly related to the $PSS(\lambda)$, and hence connected to the system energy landscape (1st z-axis). Due to the extraordinary long thermal half-lives of AAPs (\approx days), the energy state and the mechanical properties are maintained in the time frame of common experiments without the need for continued irradiation. Conceptually this goes beyond classical responsive materials, that typically only switch from state A (λ_1) to state B (λ_2), as we herein target to explore adaptation as a function of a more complex light-controlled energy landscape using widely different wavelengths.^[18]

To integrate the AAP photoswitches with controllable multivalency in the outer blocks of water-soluble star-shaped polymers, we developed a versatile polymer platform approach. Briefly, we chain-extended a 4arm-PEG (sPEG-OH, $M_n = 41\,170\text{ g mol}^{-1}$, $D = 1.04$) with active ester-containing monomers (pentafluorophenyl acrylate, PFPFA) via Radical Addition Fragmentation Transfer (RAFT) polymerization to a length of ca. 51 PFPFA (Scheme 1).^[27] Those PFPFA units were functionalized with mixtures of *p*-*iso*-propoxy-AAP-PEG-amine (iPrO-AAP-PEG) and 2-(2-aminoethoxy)ethanol, followed by end group modification (removal of the hydrophobic chain transfer agent) using 3-sulfopropyl acrylate as an

additional solubility aid (experimental details in the Supporting Information; Figure S3–5). Using this Scheme, we prepared four different multivalent star-shaped block copolymers (sPEG-AAP_x), where *x* denotes the amount of AAP units per arm (*x* ≈ 6.3, 11.7, 14.8, and 17.0). Table S1 summarizes the molecular characteristics of all sPEG-AAP_x polymers. Their well-defined nature is evident from the low dispersity *D* of 1.12–1.22, which renders them suitable to obtain conclusive structure-property relationships.

Prior to the discussion of the mechanical properties of the sPEG-AAP_x hydrogels, we discuss the switching behavior of iPrO-AAP-PEG on a molecular level by firstly analyzing the maximum switch/PSS using the two limiting wavelengths (Figure 2), and secondly by addressing the detailed adjustment of intermediate PSSs using modulated light conditions (Figure 3). For a basic characterization of the maximum PSS attainable, we irradiated a solution of iPrO-AAP-PEG (1.0 mM in D₂O) with LEDs of 375 nm and 545 nm (Figure S6,7) until the respective PSS was reached and subsequently recorded ¹H-NMR spectra (Figure 2a,b). Once a PSS is reached, iPrO-AAP-PEG maintains its *E/Z* ratio in the time frame of common experiments, because the metastable *Z*-isomer possesses a thermal half-life of $\tau_{1/2} = 5.2$ days at 25 °C and pH 7.4 (Figure S8).^[28] A thermal half-life of more than five days is a very important feature, because we later exploit this deep metastability to not only adjust the PSS, but also to maintain the system at a certain PSS without a considerable decay of the *Z*-isomer. Since the *E*- and the *Z*-isomer feature different ¹H-NMR signals (highlighted in Figure 2b), the integration of the pyrazole-methyl groups

reveals a PSS of $PSS_Z(375 \text{ nm}) = 98.4 \pm 0.4\%$ and $PSS_E(545 \text{ nm}) = 96.2 \pm 0.1\%$ after irradiation with 375 nm and 545 nm, respectively. Subsequently, we acquired UV/Vis spectra of the solutions of *E*- and *Z*-iPrO-AAP-PEG (diluted to 50 μM, pH 7.4) to correlate the absorbance at a certain wavelength to the PSS. This calibration allows later to spectroscopically determine intermediate PSSs according to Beer–Lambert law (Figure 2c). The UV/Vis spectrum of the *Z*-isomer shows that the $\pi\text{-}\pi^*$ and the $n\text{-}\pi^*$ transitions of the *Z*-isomer are well separated with a relative minimum at 372 nm (blue graph). In addition, the *E*-isomer does not absorb at wavelengths larger than 520 nm (inset, black graph), which is why iPrO-AAP-PEG features nearly quantitative photoisomerization. Calculating the difference of both UV/Vis spectra (*E*–*Z*; Figure 2d) highlights more clearly the maximum absorption differences between both isomers. The black area from 307–412 nm indicates a higher absorptivity of the *E*-isomer, while the *Z*-isomer flanks this area at both side (blue areas). The isosbestic points are highlighted by red circles (Figure 2c,d). To illustrate the robustness of iPrO-AAP-PEG as a photoswitch, we alternately irradiated the aqueous solution with 375 nm (purple background; Figure 2e) and 545 nm (green background) and determined the PSS spectroscopically. Accordingly, iPrO-AAP-PEG isomerizes nearly quantitatively over 300 switching cycles without any detectable photo-induced degradation ($\ll 1\%$), which is important for later material investigations as it confirms minimum fatigue.

Next, we turn to the detailed finetuning of the photo-switch behavior. The performance of AAP and other photo-

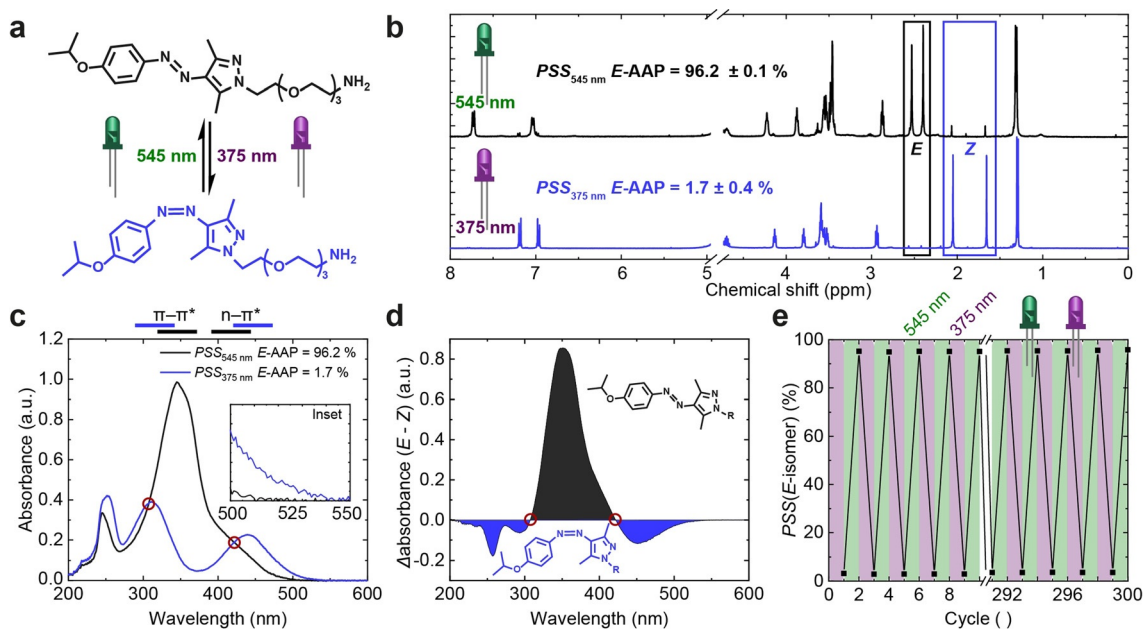


Figure 2. General photoswitch performance of *E*- and *Z*-iPrO-AAP-PEG on a molecular level. a) Schematic photoisomerization of iPrO-AAP-PEG using LEDs of the wavelength of 545 and 375 nm. b) ¹H-NMR spectra of *E*- and *Z*-iPrO-AAP-PEG in D₂O upon irradiation with 545 and 375 nm. The residual solvent peak was cut from the spectra for reasons of clarity. The PSS is calculated via the integration of the pyrazole-methyl groups. c) Corresponding UV/Vis spectra of *E*- and *Z*-iPrO-AAP-PEG at pH 7.4. The spectra show that the *E*-isomer does not absorb light with a wavelength longer than 520 nm and that the $\pi\text{-}\pi^*$ and $n\text{-}\pi^*$ transitions of the *Z*-isomer are well separated. d) The difference of both UV/Vis spectra vividly illustrates at which region of the spectrum the *E*-isomer (black area) absorbs more strongly than the *Z*-isomer (blue area) and *vice versa*. e) Photostability of iPrO-AAP-PEG. The photoswitch shows a photoinduced fatigue of $\ll 1\%$ within 300 switching cycles.

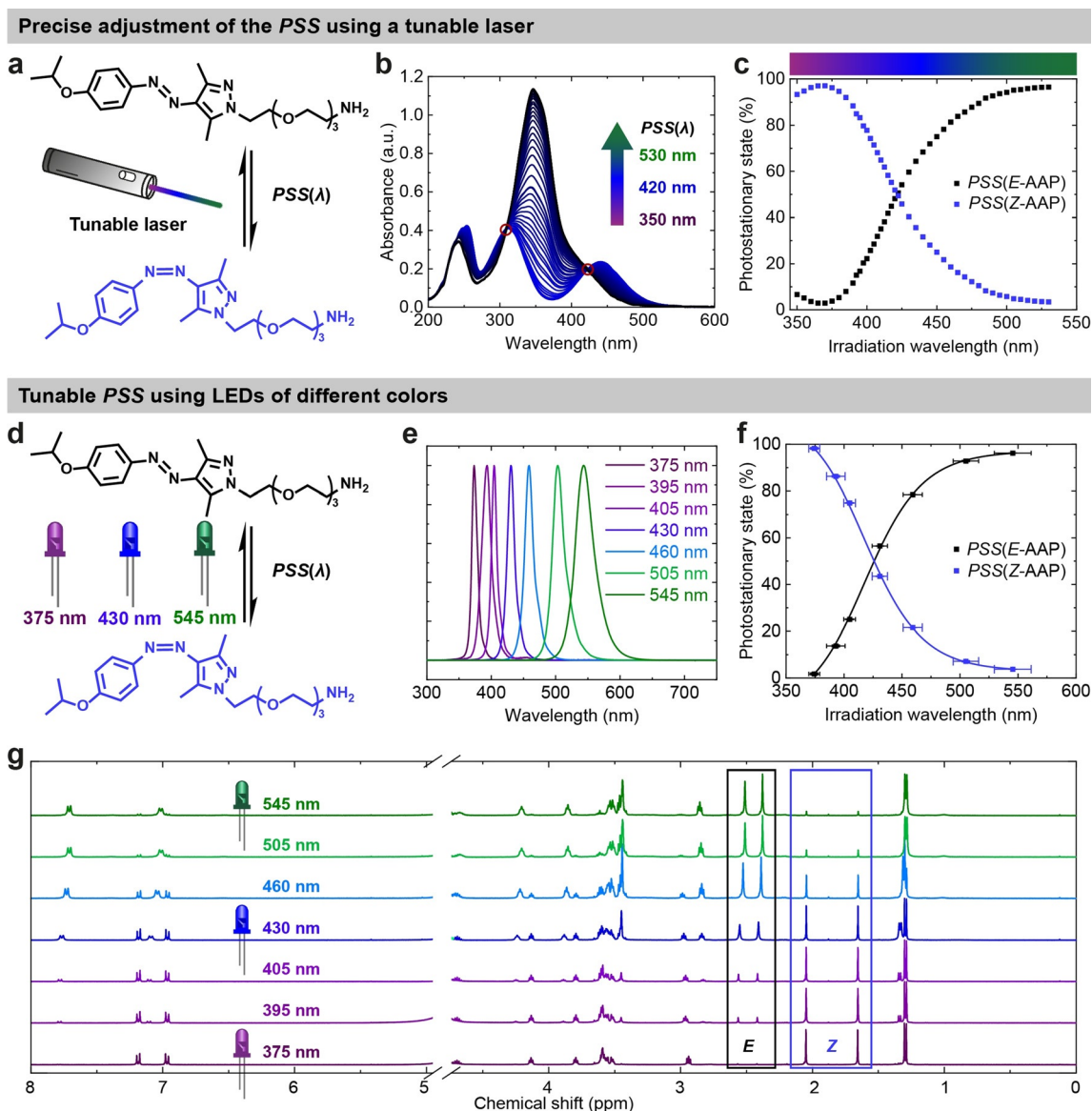


Figure 3. Tunable PSS of iPrO-AAP-PEG using different colors of light via irradiation with a tunable laser (top) and LEDs of different colors (bottom). a) Scheme of the photoisomerization of iPrO-AAP-PEG upon irradiation with a tunable laser. b) UV/Vis spectra in dependence on the irradiation wavelength. Longer irradiation wavelengths lead to higher PSSs of the *E*-isomer and *vice versa*. c) PSS as a function of the irradiation wavelength. Based on a $^1\text{H-NMR}$ calibration, the UV/Vis spectra of (b) are presented as PSS of both isomers in dependence on the irradiation wavelength. d) Schematic photoisomerization using commercial LEDs with different colors of light. e) Emission spectra of the LEDs. f) PSS as a function of the wavelengths of the LEDs. The error bars in *x*-direction are based on the emission profile of the respective LED and the ones in *y*-direction are calculated from duplicate measurements. The illustrated curves are guides to the eye. g) $^1\text{H-NMR}$ spectra in D_2O after irradiation with seven LEDs of different colors. The residual solvent peak was cut from the spectra.

switches is generally characterized by the wavelengths at which the PSSs are greatest (here, 375 nm and 545 nm). Per definition however, the PSS represents the stoichiometric composition in quasi-equilibrium of *E*- and *Z*-iPrO-AAP which are converted into each other in a reversible photochemical reaction by irradiation of *any* wavelength. Hence, we hypothesized that the PSS can in fact be tuned on-demand with light of different colors and any intermediate ratio of *E*- and *Z*-iPrO-AAP can be achieved between the two maximum PSSs (Figure 3a). To test our hypothesis of modulating the PSS to intermediate ratios, we utilized a tunable laser and

stepwise irradiated an iPrO-AAP-PEG solution ($50\ \mu\text{M}$, pH 7.4) from 350 to 530 nm inside a UV/Vis spectrometer until the equilibrated PSS was reached (see Figure S7 for experimental setup). Figure 3b displays a selection of UV/Vis spectra, that evolve continuously from nearly full *Z*-iPrO-AAP at 370 nm to nearly full *E*-iPrO-AAP at 530 nm. This clearly shows that every intermediate PSS can indeed be achieved. The highest PSSs are obtained using 370 nm and 530 nm, respectively, whereby the former corresponds very well to the relative absorption minimum of *Z*-iPrO-AAP-PEG at 372 nm (Figure 2c). Using the NMR-based calibra-

tion, it is possible to quantify the E/Z ratio. Starting from the maxima, the PSS s of both isomers show a sigmoidal dependence on the irradiation wavelength with a crossover ($PSS_E = PSS_Z = 50\%$; Figure 3c) at $\lambda_c = 421$ nm. The crossover coincides well with the isosbestic point as shown in Figure 3b (red circles). Although it appears intuitive that a PSS of 50% is reached when both isomers absorb equally, it cannot be taken for granted. The PSS depends on the quantum yield Φ

$$\Phi(\lambda, \epsilon) = \frac{\# \text{ photons inducing isomerization}}{\# \text{ photons absorbed}} \quad (1)$$

which in turn is a function of the wavelength λ and the extinction coefficient ϵ . The fact that both the isosbestic point and the crossover are found at ca. 421 nm implies that the quantum yields of both photoisomerization processes are in fact equal $\Phi_{E \rightarrow Z}(421 \text{ nm}) = \Phi_{Z \rightarrow E}(421 \text{ nm})$. Thus, referring back to Figure 2d, the highlighted areas under the curve do not only show which isomer absorbs more strongly; they also illustrate at which wavelengths the photoisomerization from E -to- Z (black area) is more pronounced than from Z -to- E (blue area) and vice versa. Moreover, Figure S9 confirms the systematic tunability of the PSS by defining rates of the photoisomerization.

While tunable lasers allow wavelength-selective tuning of the ratio of E - and Z -iPrO-AAP, they are not economic, not available to every lab and require safety precautions. To address these problems, we also used readily available and safe-to-use commercial LEDs of different colors, which gives access to a broad range of PSS s as well (Figure 3d–g). Hence, we irradiated a solution of iPrO-AAP-PEG (D_2O , 1.0 mM) with seven LEDs of different wavelengths until the respective PSS s were reached (375–545 nm; Figure 3e and Figure S6). Subsequently, we acquired 1H -NMR spectra to determine the E/Z ratio via the integration of the pyrazole-methyl groups (Figure 3g). The integration reveals that the PSS possesses a similar sigmoidal wavelength dependence when using the LEDs, hence simplifying the operation of wavelength-gated behavior to common place equipment (Figure 3f). In the following, we will continue to use the LEDs because they facilitate an easy in situ irradiation and still cover the entire range of PSS s. In control experiments we assured that irradiation of solutions with higher concentration can produce the same PSS as compared to highly diluted samples, albeit requiring longer irradiation times to reach the quasi-equilibrium PSS (Figure S10). These results allow to transfer the understanding of the precisely tunable PSS from the molecular level to the material scale.

Prior to the rheological characterization of the multivalent hydrogels, we determined the overlap concentration c^* of sPEG-OH ($c^* = 0.9$ mM; Figure S11).^[29] As a result of the chain-extension, the overlap concentration of the sPEG-AAP_x polymers is expected to be slightly lower than c^* of sPEG-OH. Thus, the supramolecular hydrogels were characterized at a molar concentration of 0.8 mM (close to c^*) to minimize chain entanglements. This allows to derive structure-property relationships, that are truly based on the adjustable intermolecular interactions and not on entangled polymer chains. Upon dissolution at the targeted concentra-

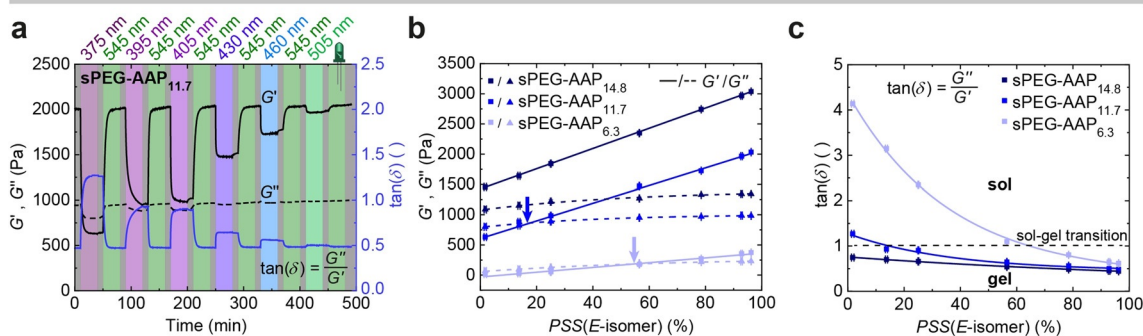
tion of 0.8 mM, the three sPEG-AAP_x polymers with $x = 6.3$, 11.7 and 14.8 AAPs units per arm form transparent hydrogels. In contrast, sPEG-AAP_{17.0} results in an opaque hydrogel, which indicates phase-separation of the outer block due to its hydrophobicity. As the macroscopic phase separation hampers to derive conclusive structure-property relationships, sPEG-AAP_{17.0} was not further considered in this study (Figure S12). Below, we will hence focus on the first three hydrogels.

At the outset, we characterized the three supramolecular hydrogels in their thermodynamic equilibrium (100% E -iPrO-AAP) from the sPEG-AAP_x via strain-sweeps in oscillatory rheology ($\gamma = 0.1$ –1000%) to determine the linear viscoelastic region (LVE: $\gamma < 20\%$; Figure S13a). To stay within the LVE, we conducted all following measurements with a strain amplitude of $\gamma = 1\%$. Within the LVE, G' and G'' increase from approximately 0.39 kPa and 0.24 kPa (sPEG-AAP_{6.3}), to 2.3 kPa and 1.3 kPa (sPEG-AAP_{11.7}), and to 3.1 kPa and 1.4 kPa (sPEG-AAP_{14.8}). The increasing stiffness is indicative of stronger multivalent interactions of E -iPrO-AAP, leading to better association. Furthermore, the frequency sweeps illustrate that sPEG-AAP_{6.3} forms a more dynamic hydrogel with a crossover frequency ($G'(f_c) = G''(f_c)$) of $f_c = 2.6$ Hz and a relaxation time ($t_{rel} = f_c^{-1}$) of $t_{rel} = 0.38$ s as opposed to sPEG-AAP_{11.7} with $f_c = 0.011$ Hz and $t_{rel} = 95$ s, respectively (Figure S13b). In contrast, the frequency sweep of sPEG-AAP_{14.8} does not show a crossover over the entire frequency range ($\omega = 0.01$ –300 rad s^{-1}) at 25 °C because of its lower dynamic character. These elementary rheological experiments of the three sPEG-AAP_x polymers confirm that the number of iPrO-AAPs per arm has a decisive influence on the mechanical properties.

In the next step, we investigated systematically, how the wavelength-dependent tunability of the ratio of E - and Z -iPrO-AAP, elucidated on the molecular level above (Figure 3), affects the hydrogel materials state. To begin with, we alternately irradiated the sPEG-AAP_{11.7} hydrogel in situ in a glass-bottom rheometer during oscillatory measurements ($\gamma = 1\%$, $\omega = 100$ rad s^{-1} , 25 °C; Figure S14) with LEDs of different colors (ranging from 375 to 505 nm) for 30 min, left the sample in the dark for 10 min, and subsequently irradiated it with green light (545 nm, 30 min). Figure 4a illustrates that the storage modulus G' and the loss modulus G'' can be precisely and reversibly tuned with the different LEDs. Longer wavelengths lead to greater moduli and vice versa. The initial irradiation with 375 nm leads to a gel-sol transition as indicated by the crossover of $G'' > G'$. Switching the material back to the E -isomer with 545 nm restores the original gel properties without a distinct deviation from the starting point. An irradiation with 395 nm, which leads to a $PSS_E(395 \text{ nm})$ of 13.7%, brings the material close to the sol-gel point. Again, the process can be reverted by 545 nm. Irradiation with the other LEDs with intermediate wavelengths (405 nm, 430 nm, 460 nm and 505 nm), then allows to tune the mechanical properties of the supramolecular hydrogels in the gel state as a function of the incident wavelength.

An increase of the AAP content in sPEG-AAP_{14.8} leads to a material that remains gel-like across all wavelengths, whereas the lower AAP content in sPEG-AAP_{6.3} shifts the

Reversible and precise tunability of hydrogel properties



Effective lifetime of load-bearing associative chains as a function of the PSS

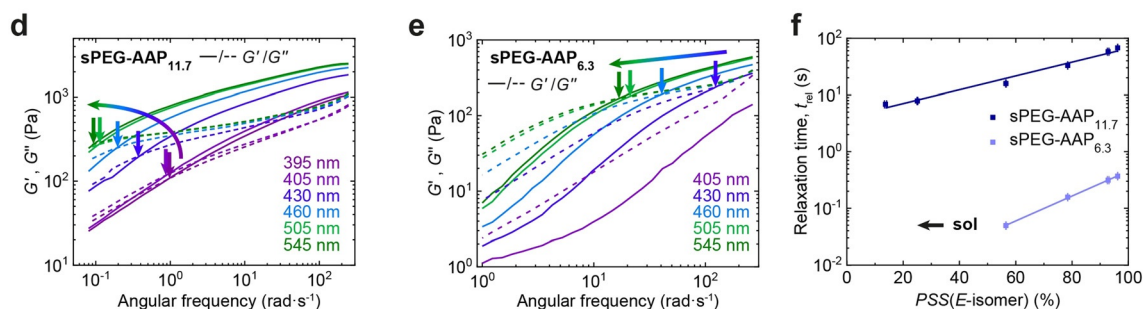


Figure 4. Rheological characteristics of the dynamically associating sPEG-AAP_x hydrogels upon irradiation with light of different wavelengths. a) Storage and loss modulus as well as the loss factor of the AAP_{11.7}-hydrogel as a function of the irradiation wavelength. Both G' and G'' increase with longer wavelengths due to stronger π - π interactions of E -iPrO-AAP, which are entirely reversible. b) Correlation between the PSS_E and the viscoelastic moduli of the three sPEG-AAP_x hydrogels. While G' correlates linearly with the PSS_E , G'' shows an exponential decay. c) Loss factor as function of the PSS_E . The loss factor decreases monotonically with an increasing PSS_E , which means that the elastic properties increase more strongly than the viscous properties with an increasing number of E -iPrO-AAP. d,e) Frequency sweeps of the dynamically associating sPEG-AAP_{11.7} and sPEG-AAP_{6.3} hydrogels. The angular crossover frequency ω_c decreases with an increasing irradiation wavelength (highlighted by arrows). f) Effective lifetime of load-bearing associative chains. The logarithmic relaxation times of both transient hydrogels depend linearly on the PSS_E , whereas the relaxation times of the sPEG-AAP_{11.7} hydrogel are approximately two orders of magnitude greater than the ones found for sPEG-AAP_{6.3}.

sol-gel transition to approximately 430 nm. Figure 4b gives detailed insights into the dependence of G' and G'' on the PSS of E -iPrO-AAP as correlated to the wavelength-dependent calibration of the PSS_E (Figure 3f). Both moduli increase with an increasing PSS_E , which confirms that E -iPrO-AAP forms stronger π - π complexes than its twisted Z -isomer. Nevertheless, the multivalent π - π interactions of Z -iPrO-AAP are still present, so that the sPEG-AAP_{14.8} hydrogel remains a gel, even upon irradiation with 375 nm ($PSS_Z = 98.3\%$). G' and G'' of the sPEG-AAP_{6.3} and the sPEG-AAP_{14.8} polymer display the exact same dependence on the PSS_E , featuring lower and higher values, respectively. Remarkably, G' correlates linearly to the PSS_E , and G'' can be accurately fitted by a monoexponential decay function. This highly programmable behavior is important for materials design and indicates a similar network topology inside the different sPEG-AAP_x hydrogels. Based on the fit functions, the gel-sol transition of the sPEG-AAP_{11.7} hydrogel is found at a PSS_E of approximately 16% (small arrow; Figure 4b). In contrast, the gel-sol transition of the more dynamic sPEG-AAP_{6.3} hydrogel takes already place at a PSS_E of approximately 54%. The least dynamic sPEG-AAP_{14.8} hydrogel does not display a gel-sol transition at a $PSS_E \geq 1.7\%$. Evidently, the aromatic interactions are dependent on the ratio of E - and

Z -iPrO-AAP, which enables a precise control over the viscoelastic properties. The loss factor $\tan(\delta)$ illustrates the ratio of viscous to elastic properties.

$$\tan(\delta) = \frac{G''}{G'} \quad (2)$$

The crossover of G' and G'' is found at $\tan(\delta) = 1$, at which a sol-gel transition takes place (dashed line; Figure 4c). The fact that $\tan(\delta)$ of the three dynamic hydrogels steadily decreases with an increasing PSS_E confirms that the elastic properties increase more strongly than the viscous properties with a higher ratio of E -iPrO-AAP. This is in line with expectations: The stronger π - π interactions stiffen the hydrogels with a greater number of E -iPrO-AAPs as opposed to the twisted Z -isomer, which impedes π - π stacking. The comparison of the three sPEG-AAP_x hydrogels reveals that the systems feature lower values of $\tan(\delta)$ for increasing numbers of AAPs per arm. Upon irradiation with 375 nm for instance, corresponding to a $PSS_E(375 \text{ nm}) = 1.7\%$, $\tan(\delta)$ decreases from 4.1 (sPEG-AAP_{6.3}) to 1.3 (sPEG-AAP_{11.7}) and to 0.74 (sPEG-AAP_{14.8}). The increase of multivalent interactions leads to an increase of the elastic properties of the resulting materials. In summary, the precise and reversible tunability of

the dynamically associating hydrogels is achieved by two factors—the number of AAPs per arm and the irradiation wavelength.

Frequency-dependent measurements give deeper insights into the effect of multivalency on the average lifetimes of the transient network linkages. The effective lifetime of network junctions is defined as the inverse crossover frequency of G' and G'' ($t_{\text{rel}} = f_c^{-1}$) at a constant strain. Since the sPEG-AAP_{14.8} does not show a frequency-dependent G'/G'' crossover in the accessible frequency regime (Figure S13), we only focused in the analysis on the relaxation behavior of the two systems undergoing gel-sol transitions and significant softening. Hence, we irradiated the samples in situ with different wavelengths until the respective PSS was reached, and subsequently acquired frequency sweeps (Figure 4 d,e). For both hydrogels, the angular crossover frequency (small arrows, $\omega_c = 2\pi f_c$) decreases with an increasing irradiation wavelength. This in turn results in relaxation times that increase with an increasing PSS_E , so that lower ratios of E -iPrO-AAPs lead to more dynamic hydrogels with less associative crosslinks and a more transient network behavior. This behavior is found as function of the PSS_E and of the functionalization density of iPrO-AAPs per arm (Figure 4 f). The relaxation times of the transient sPEG-AAP_{11.7} hydrogel range from 67 s ($PSS_E(545 \text{ nm}) = 96.2\%$) to 6.9 s ($PSS_E(395 \text{ nm}) = 13.7\%$), and are thus more than two orders of magnitude greater than the ones found for the sPEG-AAP_{6.3} hydrogel (0.37 s at a PSS of 96.2% E -iPrO-AAP). In addition, the sPEG-AAP_{6.3} polymer only forms a gel-like network at PSS s greater than approximately 50% of the E -isomer (Figure 4 f). Below 50% E -isomer, the system behaves as a viscoelastic liquid over the entire frequency range ($\omega = 1\text{--}300 \text{ rad s}^{-1}$). The analysis of the effective lifetimes of load-bearing associative chains illustrates moreover that the logarithmic relaxation times of both transient hydrogels depend linearly on the PSS_E ($\lg t_{\text{rel}} \propto PSS$; Figure 4 f). This correlation underscores the excellent tunability of such gels by light of different colors.

Furthermore, we analyzed the response of the dynamically associating sPEG-AAP_{11.7} and sPEG-AAP_{6.3} hydrogel towards the simultaneous stimulation with light and temperature. To this end, we irradiated both hydrogels in situ until the respective PSS s were reached and acquired temperature

sweeps at a constant strain and a constant frequency ($\gamma = 1\%$, $\omega = 100 \text{ rad s}^{-1}$; Figure 5,ba) with continuous irradiation. The crossovers of G' and G'' indicate the gel-sol transition temperature as highlighted by small arrows. While having in mind that the crossover of G' and G'' depends on the applied frequency at a certain strain, we kept the strain and the frequency constant at this point, because it provides a basis for comparison of the hydrogels. In case of the sPEG-AAP_{11.7} hydrogel, the gel-sol transition temperature varies from ca. 80 °C after irradiation with 545 nm to ca. 39 °C after irradiation with 395 nm (Figure 5 a). Upon irradiation with 375 nm, the sPEG-AAP_{11.7} polymer behaves as a viscoelastic liquid over the entire temperature range (5–80 °C). The number of E -iPrO-AAPs ($PSS_E(375 \text{ nm}) = 1.7\%$) is too low and the dynamics are too high to form a percolating network, even at 5 °C. The more dynamic sPEG-AAP_{6.3} hydrogel features similarly wavelength-tunable gel-sol transition temperatures from ca. 48 °C (545 nm) to ca. 27 °C (460 nm). At a wavelength of 405 nm and below, the sPEG-AAP_{6.3} polymer does not form a gel over the entire temperature range (5–60 °C; Figure 5 b). Remarkably, the gel-sol transition temperatures of both hydrogel depend linearly on the PSS of E -iPrO-AAP, whereby the slope of both linear regressions is approximately 0.5 K %⁻¹ (Figure 5 c). The similar slopes indicate a very similar network topology in the gels. This correlation additionally confirms how precisely the mechanical properties of such sPEG-AAP_x hydrogels can be tuned by the incident wavelength and represents a promising approach for prospective adaptive materials with spatiotemporally controlled gel-sol transition temperatures.

Conclusion

We introduced a new concept for the wavelength-gated adaptation of hydrogel properties based on the multivalent interactions of photo-responsive stickers in networks via weakly associating star polymers. The material design enables to reversibly induce gel-sol transitions and to precisely tune the stiffness of hydrogels as a function of the number of AAPs and on the wavelength of the incident light. These parameters concurrently allow to engineer the dynamics of the network in terms of the effective lifetime of load-bearing associative

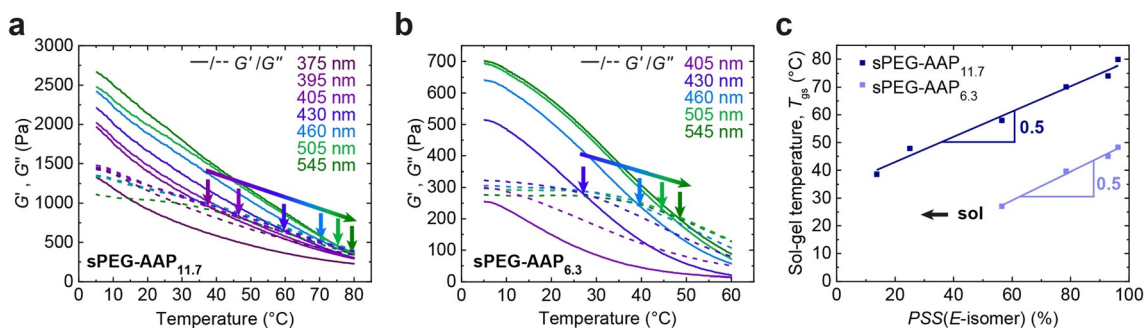


Figure 5. Wavelength-gated gel-sol transition temperature of a) sPEG-AAP_{11.7} and b) sPEG-AAP_{6.3}. The crossovers of G' and G'' are highlighted by small arrows. The gel-sol transition temperatures vary from 80 °C (545 nm) to 39 °C (395 nm) for the sPEG-AAP_{11.7} hydrogel and from 48 °C (545 nm) to 27 °C (460 nm) for the sPEG-AAP_{6.3} hydrogel. c) Linear dependence of the sol-gel temperature, T_{gs} , on the PSS_E . The slope of both linear regressions is approximately 0.5 K %⁻¹.

chains and its gel-sol transition temperature. The remarkable self-similar behavior between polymers of different functionalization density with respect to distinct structure/*PSS*/material property relationships ($G' \propto PSS$; $G'' \propto \exp(-PSS)$; $\lg t_{rel} \propto PSS$, $T_{gs} \propto 0.5 PSS$) allows for a desirable and deterministic photo-adaptive materials design. It raises the relevant questions to what extent this behavior can be generalized to other supramolecular interactions.

The foundation of the wavelength-gated engineering on the material scale relies on a multivalent approach in correlation to the thorough calibration of the *PSS* of iPrO-AAP on the molecular level. The precise calibration to tune the ratio of *E*-/*Z*-iPrO-AAP translates to the reversible modulation of the mechanical characteristics of the hydrogels in a spatiotemporal fashion. Any intermediate *E*/*Z* ratio can be obtained with a tunable laser, but also cost-efficient LEDs cover the entire range of *PSS*s, rendering the approach of a tunable *PSS* suitable for broader field of research and application. Moreover, the used photoswitch facilitates to maintain the mechanical properties since its thermal relaxation can be neglected in the time frame of common experiments.

The introduced approach of a wavelength-gated adaptation of hydrogel properties goes beyond the classical switching from state A to state B. Considering stem cell culturing for instance, in which the hydrogel stiffness and viscoelastic properties regulate stem cell fate and tissue formation, the mechanical properties of the hydrogel support can be adjusted on-demand, and, more importantly, with wavelengths outside the harmful UV regime. Thus, the approach of a wavelength-gated engineering paves the way for prospective adaptive materials with advanced and tunable properties in cell culturing, tissue engineering and 3D bioprinting.

Acknowledgements

We acknowledge funding from the Volkswagen Foundation (A125456) and the SFB 985 "Functional Microgels and Microgel Systems" (Project C4). A.W. thanks the DFG for financing NMR instrumentation that is operated within the MagRes Center of the University of Freiburg. A.W. thanks MPI Minerva Foundation for an ARCHES Award. Open access funding enabled and organized by Projekt DEAL.

Conflict of interest

The authors declare no conflict of interest.

Keywords: Arylazopyrazole · Hydrogels · Photoresponsive Systems · Photoswitch · Wavelength-Gated Engineering

- [1] G. A. Parada, X. Zhao, *Soft Matter* **2018**, *14*, 5186–5196.
[2] T. Heuser, E. Weyandt, A. Walther, *Angew. Chem. Int. Ed.* **2015**, *54*, 13258–13262; *Angew. Chem.* **2015**, *127*, 13456–13460.

- [3] S. Burattini, B. W. Greenland, D. H. Merino, W. Weng, J. Seppala, H. M. Colquhoun, W. Hayes, M. E. Mackay, I. W. Hamley, S. J. Rowan, *J. Am. Chem. Soc.* **2010**, *132*, 12051–12058.
[4] K. A. Günay, T. L. Ceccato, J. S. Silver, K. L. Bannister, O. J. Bednarski, L. A. Leinwand, K. S. Anseth, *Angew. Chem. Int. Ed.* **2019**, *58*, 9912–9916; *Angew. Chem.* **2019**, *131*, 10017–10021.
[5] F. Mayer, S. Richter, J. Westhauser, E. Blasco, C. Barner-Kowollik, M. Wegener, *Sci. Adv.* **2019**, *5*, eaau9160.
[6] R. Batchelor, T. Messer, M. Hippler, M. Wegener, C. Barner-Kowollik, E. Blasco, *Adv. Mater.* **2019**, *31*, 1904085.
[7] T. E. Brown, K. S. Anseth, *Chem. Soc. Rev.* **2017**, *46*, 6532–6552.
[8] R. Eelkema, A. Pich, *Adv. Mater.* **2020**, *32*, 1906012.
[9] F. M. Yavitt, T. E. Brown, E. A. Hushka, M. E. Brown, N. Gjorevski, P. J. Dempsey, M. P. Lutolf, K. S. Anseth, *Adv. Mater.* **2020**, *32*, 1905366.
[10] a) M. Golkaram, K. Loos, *Macromolecules* **2019**, *52*, 9427–9444; b) G. Creusen, A. Roshanasan, J. G. Lopez, K. Peneva, A. Walther, *Polym. Chem.* **2019**, *10*, 3740.
[11] K. Liu, S. M. Mihaila, A. Rowan, E. Oosterwijk, P. H. J. Kouwer, *Biomacromolecules* **2019**, *20*, 826–834.
[12] J. A. McCune, S. Mommer, C. C. Parkins, O. A. Scherman, *Adv. Mater.* **2020**, *32*, 1906890.
[13] a) Y. Gu, E. A. Alt, H. Wang, X. Li, A. P. Willard, J. A. Johnson, *Nature* **2018**, *560*, 65–69; b) I. N. Lee, O. Dobre, D. Richards, C. Ballestrem, J. M. Curran, J. A. Hunt, S. M. Richardson, J. Swift, L. S. Wong, *ACS Appl. Mater. Interfaces* **2018**, *10*, 7765–7776; c) Q. M. Zhang, X. Li, M. R. Islam, M. Wei, M. J. Serpe, *J. Mater. Chem. C* **2014**, *2*, 6961–6965.
[14] M. Hörner, K. Raute, B. Hummel, J. Madl, G. Creusen, O. S. Thomas, E. H. Christen, N. Hotz, R. J. Gübeli, R. Engesser, B. Rebmann, J. Lauer, B. Rolauuffs, J. Timmer, W. W. A. Schamel, J. Pruszk, W. Römer, M. D. Zurbriggen, C. Friedrich, A. Walther, S. Minguet, R. Sawarkar, W. Weber, *Adv. Mater.* **2019**, *31*, 1806727.
[15] K. Iwaso, Y. Takashima, A. Harada, *Nat. Chem.* **2016**, *8*, 625–632.
[16] a) A. Goulet-Hanssens, F. Eisenreich, S. Hecht, *Adv. Mater.* **2020**, *32*, 1905966; b) P. Weis, S. Wu, *Macromol. Rapid Commun.* **2018**, *39*, 1700220.
[17] a) K. Han, D. Go, T. Tigges, K. Rahimi, A. J. C. Kuehne, A. Walther, *Angew. Chem. Int. Ed.* **2017**, *56*, 2176–2182; *Angew. Chem.* **2017**, *129*, 2208–2214; b) A. M. Rosales, K. M. Mabry, E. M. Nehls, K. S. Anseth, *Biomacromolecules* **2015**, *16*, 798–806.
[18] A. Walther, *Adv. Mater.* **2019**, *31*, 1905111.
[19] M. Reynders, B. S. Matsuura, M. Bérouti, D. Simoneschi, A. Marzio, M. Pagano, D. Trauner, *Sci. Adv.* **2020**, *6*, eaay5064.
[20] a) K. Kalayci, H. Frisch, C. Barner-Kowollik, V. X. Truong, *Adv. Funct. Mater.* **2020**, *30*, 1908171; b) H. A. Houck, E. Blasco, F. E. Du Prez, C. Barner-Kowollik, *J. Am. Chem. Soc.* **2019**, *141*, 12329–12337.
[21] D. Bléger, J. Schwarz, A. M. Brouwer, S. Hecht, *J. Am. Chem. Soc.* **2012**, *134*, 20597–20600.
[22] M. Kathan, S. Hecht, *Chem. Soc. Rev.* **2017**, *46*, 5536–5550.
[23] C. E. Weston, R. D. Richardson, P. R. Haycock, A. J. White, M. J. Fuchter, *J. Am. Chem. Soc.* **2014**, *136*, 11878–11881.
[24] a) L. Stricker, E.-C. Fritz, M. Peterlechner, N. L. Doltsinis, B. J. Ravoo, *J. Am. Chem. Soc.* **2016**, *138*, 4547–4554; b) L. Stricker, M. Böckmann, T. M. Kirse, N. L. Doltsinis, B. J. Ravoo, *Chem. Eur. J.* **2018**, *24*, 8639–8647; c) C. W. Chu, L. Stricker, T. M. Kirse, M. Hayduk, B. J. Ravoo, *Chem. Eur. J.* **2019**, *25*, 6131–6140.
[25] a) Z. Du, B. Ren, X. Chang, R. Dong, J. Peng, Z. Tong, *Macromolecules* **2016**, *49*, 4978–4988; b) V. Metri, A. Louhichi, J. Yan, G. P. Baeza, K. Matyjaszewski, D. Vlassopoulos, W. J. Briels, *Macromolecules* **2018**, *51*, 2872–2886.

- [26] S. Crespi, N. A. Simeth, B. König, *Nat. Rev. Chem.* **2019**, *3*, 133–146.
- [27] D. Hoenders, T. Tigges, A. Walther, *Polym. Chem.* **2015**, *6*, 476–486.
- [28] S. Ludwanowski, M. Ari, K. Parison, S. Kalthoum, P. Straub, N. Pompe, S. Weber, M. Walter, A. Walther, *Chem. Eur. J.* **2020**, *26*, 13203–13212.
- [29] T. Sakai, T. Matsunaga, Y. Yamamoto, C. Ito, R. Yoshida, S. Suzuki, N. Sasaki, M. Shibayama, U.-i. Chung, *Macromolecules* **2008**, *41*, 5379–5384.

Manuscript received: August 24, 2020

Revised manuscript received: October 23, 2020

Accepted manuscript online: November 12, 2020

Version of record online: December 21, 2020